Optimal Frequency for Wireless Power Transmission Into Dispersive Tissue

Ada S. Y. Poon, *Member, IEEE*, Stephen O'Driscoll, *Member, IEEE*, and Teresa H. Meng, *Fellow, IEEE*

***Abstract*—RF wireless interface enables remotely-powered implantable devices. Current studies in wireless power transmission into biological tissue tend to operate below 10 MHz due to tissue absorption loss, which results in large receive antennas. This paper examines the range of frequencies that will optimize the tradeoff between received power and tissue absorption. It first models biological tissue as a dispersive dielectric in a homogeneous medium and performs full-wave analysis to show that the optimal frequency is above 1 GHz for small receive coil and typical transmit-receive separations. Then, it includes the air-tissue interface and models human body as a planarly layered medium. The optimal frequency is shown to remain in the GHz-range. Finally, electromagnetic simulations are performed to include the effect of load impedance and look at the matched power gain. The optimal frequency is in the GHz-range for mm-sized transmit antenna and shifts to the sub-GHz range for cm-sized transmit antenna. The multiple orders of magnitude increase in the operating frequency enables dramatic miniaturization of implantable devices.**

***Index Terms*—Implantable medical devices, wireless power transfer.**

I. Introduction

IMPLANTABLE medical devices will play an important role in modern medicine for preventive and post-surgery monitoring, drug delivery, local stimulation, and biomimetic prosthesis. To reduce the risk of wire snapping, and replacement and corrosion of embedded batteries, wireless delivery of energy to these devices is desirable. Low-frequency electromagnetic field as the carrier in conjunction with inductive coupling as the transmission mechanism is a commonly used approach. In the past fifty years, analyses [1]–[5], circuit design techniques [4], [6]–[11], link optimization [12], and prototype implementations [13]–[16] tended to operate at frequencies below 10 MHz. On the other hand, the telemetry systems, either battery powered or wirelessly powered by a low-frequency carrier, operate between 10 MHz to a few GHz [17]–[20]. In a related field to wireless power delivery, thermotherapy where electromagnetic field is used to heat up a targeted area inside the body such as hyperthermia, uses both low-frequency (<10 MHz) and high-frequency (>1 GHz) carriers ([21], Ch. 4). Work has been done on identifying the frequency that optimizes the tradeoff between penetration and resolution [22]. A fundamental question therefore arises: is there an optimal frequency for the wireless delivery of power into biological tissue that maximizes the ratio of received power to total tissue absorption? In this paper, we consider the scenario where the receiver dimension is much smaller than its depth inside the body, and show that there exists an optimal frequency and this frequency is in the sub-GHz to the low GHz-range.

Let us first review the reasoning behind the popular use of low-frequency carrier in wireless power transmission. As tissue absorption increases with frequency, most analyses assume that lower frequency would yield better transfer efficiency. They therefore omit the displacement current. The propagation of electromagnetic field is then governed by a diffusion equation which is a quasi-static approximation to Maxwell's equations. Solving the diffusion equation reveals that electromagnetic fields decay exponentially inside tissue and the length of diffusion is inversely proportional to the square root of frequency. That is, higher frequency decays faster which agrees with the initial assumption and reinforces the use of low-frequency carrier. However, the diffusion equation is a valid approximation for good conductors, and tissue is better modeled as a low loss dielectric in which displacement current is significant. Solving the Helmholtz equation reveals that the penetration depth is asymptotically independent of frequency at high frequency. As received power is proportional to the rate of change of the incident magnetic field, higher carrier frequency is seemingly better. However, dielectric dispersion in tissue begins to play a role in the GHz-range. Therefore, we conjecture the existence of an optimal frequency.

To find the optimal frequency, we will first model biological tissue as a dispersive dielectric in a homogeneous medium, and approximate the transmitted field by the field emanated from the set of lowest order magnetic multipoles. Here, we define the power transfer efficiency as the ratio of received power to total tissue absorption. For a small receive coil, the frequency that optimizes this efficiency, is shown to be

$$f_{\text{opt}} \approx \frac{1}{2\pi}\sqrt{\frac{c\sqrt{\epsilon_{r0}}}{d\tau(\epsilon_{r0}-\epsilon_{\infty})}} \tag{1}$$

where $(\epsilon_{r0}, \epsilon_{\infty}, \tau)$ characterizes the dielectric properties of tissue in the Debye relaxation model and d is the transmit-receive separation. Based on the measured data in [23], the optimal frequencies for 17 different kinds of biological tissue

Manuscript received March 08, 2008; revised September 07, 2009, accepted November 29, 2009. Date of publication March 01, 2010; date of current version May 05, 2010. This paper was presented in part at the Annual International Conference of the IEEE Engineering in Medicine and Biology Society, Lyon, France, Aug. 23–26, 2007 and also at the IEEE International Solid-State Circuits Conference, San Francisco, CA, Sep. 2–6, 2009.

A. S. Y. Poon and T. H. Meng are with the Department of Electrical Engineering, Stanford University, CA 94305 USA (e-mail: adapoon@stanford.edu; thm@stanford.edu).

S. O'Driscoll is with the Department of Electrical and Computer Engineering, University of California, Davis, CA 95616 USA (e-mail: odriscoll@ucdavis.edu).

Color versions of one or more of the figures in this paper are available online at http://ieeexplore.ieee.org.

Digital Object Identifier 10.1109/TAP.2010.2044310

are above 1 GHz even for a separation of 10 cm. The transfer efficiency at the optimal frequency is approximately proportional to $(1)/(d^3)$. This implies that the regime for optimal power transmission is in between the far field and the near field.

Next, we include the air-tissue interface and model human body as a planarly layered medium, and replace the source model by a finite dimensional current loop. We compute the Sommerfeld integrals and show that the optimal frequency remains in the GHz-range for typical tissue composition and transmit-receive separation. We also perform the SAR (specific absorption rate) calculation and compute the maximum induced voltage at the receiver. Depending on the load impedance, sub-mW to mW of power can be safely delivered to a mm-sized receive coil from a cm-sized transmit coil with a separation of a few cm at carrier frequency of 1 GHz.

Lastly, as received power depends on the load impedance, we will study its effect on the optimal frequency. The choice of load impedance depends on receiver design. In the inductively coupled link, resonant tuning is a commonly used technique [1]–[16]. The load impedance is chosen to achieve a given output voltage. The tuning configuration—series versus shunt tuning—is chosen to maximize the overall power gain. Shunt tuning at receiver and series tuning at transmitter is the most commonly used configuration. As our objective is to achieve maximum power transfer efficiency, a different approach is to model the power link as a two-port network and perform simultaneously conjugate matching at the transmitter and the receiver. The output voltage requirement is then fulfilled by the choice of various matching networks. We will include the matching network and perform electromagnetic simulation using Zeland IE3D [24]. The optimal frequency is in the GHz-range for mm-sized transmit coil and shifts to the sub-GHz range for cm-sized transmit coil.

We progressively include the effect of tissue dielectric properties, air-tissue multi-layered structure, and load impedance at the receiver, and study their effect on the optimal frequency for power transmission. All the results suggest that the optimal frequency is about 2 order of magnitude higher than the commonly used range of frequencies. For a fixed power transfer efficiency, the dimension of the receiver can be reduced by 100 times. This allows dramatic miniaturization of implantable devices. Furthermore, higher carrier frequency has better tolerance to receiver displacement and orientation. If data is modulated on top of the power carrier, wider signal bandwidth and hence higher data rate can be supported.

The rest of the paper is organized as follows. Section II presents the model and problem formulation. Sections III, IV, and V investigate the effect of dielectric dispersion in tissue, layered structure of body, and load impedance at receiver on the optimal frequency respectively. Finally, we conclude this paper in Section VI.

In the following, we use boldface letters for vectors and boldface capital letters with a bar such as $\bar{\mathbf{G}}$ for matrices. For a vector $\mathbf{r}, r$ denotes its magnitude and $\hat{\mathbf{r}}$ is a unit vector denoting its direction. $(\cdot)^*$ and $(\cdot)^\dagger$ denotes the conjugate and the conjugate transpose operations respectively. For a complex number $z, \mathrm{Re}\ z$ and $\mathrm{Im} z$ denote the real and the imaginary parts respectively.

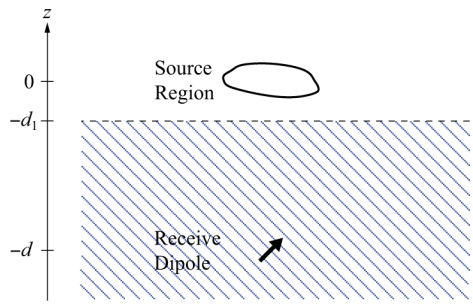

Fig. 1. A source region on top of an arbitrary oriented receive dipole.

II. Model and Problem Formulation

Referring to Fig. 1, we consider a source region of magnetic current density delivering power to an arbitrarily oriented magnetic dipole. First, we consider a source region despite the fact that most study in the literature models the penetration of electromagnetic field into tissue as a plane wave normally incident on the air-tissue interface. It is because the source region is close to the tissue and the separation is usually much less than a wavelength. Thus, the plane-wave model is not appropriate. Second, only solenoidal current sources are used because their electric near field is smaller. Therefore, tissue absorption is less. Similar argument is made in [25]. Third, we consider area-constrained implantable devices and therefore we model the receive antenna as a magnetic dipole.

Assuming all sources and fields have a time dependence $e^{-i\omega t}$, the electromagnetic fields due to the transmit magnetic current density $\mathbf{M}_{tx}(\mathbf{r})$ and the induced receive current density $\mathbf{M}_{rx}(\mathbf{r})$ satisfy

$$\nabla \times \mathbf{H} = -i\omega\epsilon\mathbf{E} \tag{2a}$$

$$\nabla \times \mathbf{E} = i\omega\mu_0\mathbf{H} - \mathbf{M}_{tx} - \mathbf{M}_{rx}. \tag{2b}$$

Substituting them into the Poynting theorem yields

$$\nabla\cdot(\mathbf{E}\times\mathbf{H}^*) = i\omega\mu_0|\mathbf{H}|^2 - i\omega\epsilon^*|\mathbf{E}|^2 - \mathbf{H}^* \cdot\mathbf{M}_{tx} - \mathbf{H}^*\cdot\mathbf{M}_{rx}. \tag{3}$$

Rearranging terms, the transmitted power density is related to the received power density and losses by

$$-\mathbf{H}^*\cdot\mathbf{M}_{tx} = \nabla\cdot(\mathbf{E}\times\mathbf{H}^*) - i\omega\mu_0|\mathbf{H}|^2 + i\omega\epsilon^*|\mathbf{E}|^2 + \mathbf{H}^*\cdot\mathbf{M}_{rx}. \tag{4}$$

The term on the left is the complex transmitted power density. On the right, $\nabla\cdot(\mathbf{E}\times\mathbf{H}^*)$ is the radiation loss; the imaginary part of $\omega\epsilon^*|\mathbf{E}|^2$ is the sum of dielectric loss and induced-current loss; and $\mathbf{H}^*\cdot\mathbf{M}_{rx}$ is the complex received power density. Suppose d_1 is the distance between the center of the source region and the tissue interface. Then, the tissue region is defined by $z < -d_1$ and the amount of energy absorbed by the tissue is

$$P_{\mathrm{loss}} := \frac{\omega}{2}\int_{z<-d_1} \mathrm{Im}\,\epsilon(\mathbf{r})|\mathbf{E}(\mathbf{r})|^2\,d\mathbf{r}. \tag{5}$$

Suppose the receive dipole is at $-\hat{\mathbf{z}}d$ and is pointing in the direction $\hat{\mathbf{n}}$. The power transferred to the receive dipole is given by

$$P_r := \mathrm{Re}\left\{\frac{1}{2}\,\mathbf{H}^*(-\hat{\mathbf{z}}d)\cdot(-i\omega\mu_0 I_r A_r\hat{\mathbf{n}})\right\} \tag{6}$$

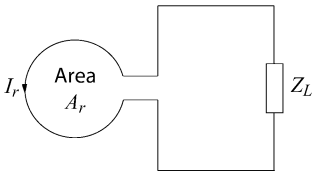

Fig. 2. A receive current loop connected to a load Z_L.

where I_r is the induced current on the receive dipole and A_r is the area of the dipole. As we are concerned with the amount of heat absorbed by the tissue, we define the power transfer efficiency as the ratio of real received power to total tissue absorption:

$$\eta := \frac{P_r}{P_{\text{loss}}}. \tag{7}$$

The scattered field due to the induced current density $\mathbf{M}_{rx}$ is much weaker than the incident field due to $\mathbf{M}_{tx}$. Therefore, the electromagnetic fields can be approximated by ignoring the scattered field. Then, the fields can be expressed in integral forms as

$$\mathbf{H}(\mathbf{r}) = i\omega\epsilon(\mathbf{r}) \int \bar{\mathbf{G}}_m(\mathbf{r},\mathbf{r}')\mathbf{M}_{tx}(\mathbf{r}')\, d\mathbf{r}' \tag{8a}$$

$$\mathbf{E}(\mathbf{r}) = -\int \bar{\mathbf{G}}_e(\mathbf{r},\mathbf{r}')\mathbf{M}_{tx}(\mathbf{r}') \tag{8b}$$

where $\bar{\mathbf{G}}_m(\mathbf{r},\mathbf{r}')$ and $\bar{\mathbf{G}}_e(\mathbf{r},\mathbf{r}')$ are the magnetic and the electric dyadic Green functions respectively. Different transmission media will have different sets of Green functions. In the next two sections, we will study the variation of η with frequency in homogeneous and planarly layered media.

Finally, the total magnetic flux incident on the receive dipole is $\mu_0\mathbf{H}(-\hat{\mathbf{z}}d)\cdot\hat{\mathbf{n}}A_r$. The rate of change of this total flux yields the induced emf. With reference to Fig. 2, this induced emf is the voltage across the load impedance Z_L and hence, the induced current I_r equals to $i\omega\mu_0\mathbf{H}(-\hat{\mathbf{z}}d)\cdot\hat{\mathbf{n}}A_r/Z_L$. The received power can be written as

$$P_r = \frac{\omega^2\mu_0^2 A_r^2 \text{Re}\frac{1}{Z_L}}{2}|\mathbf{H}(-\hat{\mathbf{z}}d)\cdot\hat{\mathbf{n}}|^2. \tag{9}$$

In the next two sections, we will assume a fixed load impedance while in Section V, we will study the variation of η with frequency for matched load.

III. Optimal Frequency in Homogeneous Dispersive Tissue

This section investigates the effect of dielectric dispersion in tissue. Therefore, we assume the medium is homogeneous with $\epsilon(\mathbf{r}) = \epsilon_0\epsilon_r$ and the tissue dispersion is captured by the frequency variation of the relative permittivity ϵ_r. We decompose the dyadic Green functions into a sum of vector multipoles. In a homogeneous medium and spherical coordinates (r,θ,ϕ), these multipoles are given by [26, Ch. 7]

$$\boldsymbol{\xi}_{nm}(\mathbf{r}) = \nabla\times\left[\mathbf{r}h_n^{(1)}(kr)Y_{nm}(\theta,\phi)\right] \tag{10a}$$

$$\boldsymbol{\psi}_{nm}(\mathbf{r}) = \frac{1}{k}\nabla\times\nabla\times\left[\mathbf{r}h_n^{(1)}(kr)Y_{nm}(\theta,\phi)\right] \tag{10b}$$

$$\tilde{\boldsymbol{\psi}}_{nm}(\mathbf{r}) = \frac{1}{k}\nabla\times\nabla\times[\mathbf{r}j_n(kr)Y_{nm}^*(\theta,\phi)] \tag{10c}$$

where $k = \omega\sqrt{\mu_0\epsilon_0\epsilon_r}$, $h_n^{(1)}(r)$ is the spherical Hankel function of the first kind, $j_n(r)$ is the spherical Bessel function, and $Y_{nm}(\theta,\phi)$ is the spherical harmonic function of degree n and order m using the Schmidt seminormalized definition. The Green functions can then be written as

$$\bar{\mathbf{G}}_m(\mathbf{r},\mathbf{r}') = \frac{ik}{4\pi}\sum_{n=1}^{\infty}\sum_{m=-n}^{n}\frac{2n+1}{n(n+1)}\boldsymbol{\psi}_{nm}(\mathbf{r})\tilde{\boldsymbol{\psi}}_{nm}(\mathbf{r}') \tag{11a}$$

$$\bar{\mathbf{G}}_e(\mathbf{r},\mathbf{r}') = \frac{ik^2}{4\pi}\sum_{n=1}^{\infty}\sum_{m=-n}^{n}\frac{2n+1}{n(n+1)}\boldsymbol{\xi}_{nm}(\mathbf{r})\tilde{\boldsymbol{\psi}}_{nm}(\mathbf{r}'). \tag{11b}$$

Electromagnetic fields at a distance $\mathbf{r}$ depend on the source $\mathbf{M}_{tx}(\mathbf{r}')$ from its projection onto $\tilde{\boldsymbol{\psi}}_{nm}(\mathbf{r}')$'s. For a small source region, the projection onto the lowest order multipoles $(n=1)$ suffice to model the source region. The corresponding electromagnetic fields are given by

$$\mathbf{H}(\mathbf{r}) = \frac{ik^3}{4\pi}\left[\alpha_{-1}\boldsymbol{\psi}_{1,-1}(\mathbf{r}) + \alpha_0\boldsymbol{\psi}_{1,0}(\mathbf{r}) + \alpha_1\boldsymbol{\psi}_{1,1}(\mathbf{r})\right] \tag{12a}$$

$$\mathbf{E}(\mathbf{r}) = \frac{\omega\mu_0 k^2}{4\pi}[\alpha_{-1}\boldsymbol{\xi}_{1,-1}(\mathbf{r}) + \alpha_0\boldsymbol{\xi}_{1,0}(\mathbf{r}) + \alpha_1\boldsymbol{\xi}_{1,1}(\mathbf{r})]. \tag{12b}$$

The direction of $((\alpha_{-1}-\alpha_1)/(\sqrt{2}), (\alpha_{-1}+\alpha_1)/(\sqrt{2}), \alpha_0)$ gives the orientation of the transmit dipole and its magnitude $\sqrt{|\alpha_{-1}|^2+|\alpha_0|^2+|\alpha_1|^2}$ yields the transmit magnetic moment.

With this simplification, the integral in the tissue absorption in (5) can be expressed as

$$\int_{z<-d_1}|\mathbf{E}(\mathbf{r})|^2 d\mathbf{r} = \frac{\omega^2\mu_0^2|k|^4}{16\pi^2}\int_{z<-d_1}|\alpha_{-1}\boldsymbol{\xi}_{1,-1}(\mathbf{r}) + \alpha_0\boldsymbol{\xi}_{1,0}(\mathbf{r}) + \alpha_1\boldsymbol{\xi}_{1,1}(\mathbf{r})|^2 d\mathbf{r} \tag{13}$$

$$= \frac{\omega^2\mu_0^2|k|^4}{16\pi^2}\int_{z<-d_1}|\alpha_{-1}|^2|\boldsymbol{\xi}_{1,-1}(\mathbf{r})|^2 + |\alpha_0|^2|\boldsymbol{\xi}_{1,0}(\mathbf{r})|^2 + |\alpha_1|^2|\boldsymbol{\xi}_{1,1}(\mathbf{r})|^2\, d\mathbf{r} \tag{14}$$

in which the cross terms are zero due to the symmetry of $\boldsymbol{\xi}_{1,m}(\mathbf{r})$ in ϕ over the domain of integration. Defining $\mathbf{x}$ as a 3×1 vector with elements $\{\alpha_{-1},\alpha_0,\alpha_1\}$ and $\bar{\mathbf{K}}$ as a 3×3 diagonal matrix with diagonal elements $\{\int_{z<-d_1}|\boldsymbol{\xi}_{1,-1}(\mathbf{r})|^2\, d\mathbf{r}, \int_{z<-d_1}|\boldsymbol{\xi}_{1,0}(\mathbf{r})|^2\, d\mathbf{r}, \int_{z<-d_1}|\boldsymbol{\xi}_{1,1}(\mathbf{r})|^2\, d\mathbf{r}\}$, we have the following compact representation for the tissue absorption

$$P_{\text{loss}} = \frac{\omega^3\mu_0^2\epsilon_0\text{Im}\epsilon_r|k|^4}{32\pi^2}\mathbf{x}^\dagger\bar{\mathbf{K}}\mathbf{x}. \tag{15}$$

When the domain of integration is not a half space, $\bar{\mathbf{K}}$ can be non-diagonal but the matrix representation remains hold. Similarly, we define

$$\mathbf{h} = \begin{bmatrix}\boldsymbol{\psi}_{1,-1}^*(-\hat{\mathbf{z}}d)\cdot\hat{\mathbf{n}}\\ \boldsymbol{\psi}_{1,0}^*(-\hat{\mathbf{z}}d)\cdot\hat{\mathbf{n}}\\ \boldsymbol{\psi}_{1,1}^*(-\hat{\mathbf{z}}d)\cdot\hat{\mathbf{n}}\end{bmatrix} \tag{16}$$

the received power in matrix form is

$$P_r = \frac{\omega^2\mu_0^2 A_r^2\text{Re}\frac{1}{Z_L}|k|^6}{32\pi^2}\mathbf{x}^\dagger\mathbf{h}\mathbf{h}^\dagger\mathbf{x}. \tag{17}$$

Putting together, the power transfer efficiency can be expressed as

$$\eta = \frac{|k|^2 A_r^2\text{Re}\frac{1}{Z_L}}{\omega\epsilon_0\text{Im}\epsilon_r}\frac{\mathbf{x}^\dagger\mathbf{h}\mathbf{h}^\dagger\mathbf{x}}{\mathbf{x}^\dagger\bar{\mathbf{K}}\mathbf{x}}. \tag{18}$$

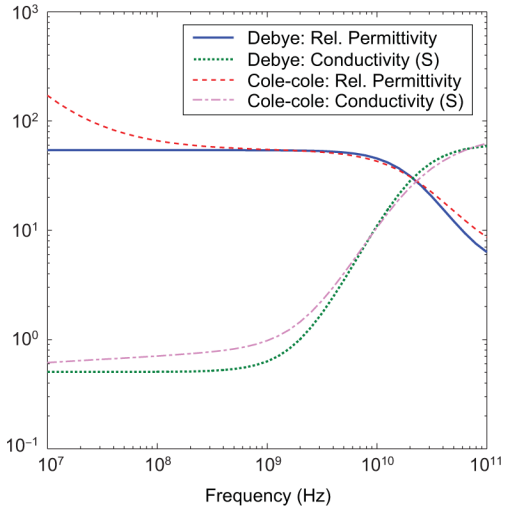

Fig. 3. Plot the real part of the relative permittivity and conductivity of muscle based on the Debye and the 4-term Cole-Cole relaxation models.

Now, the efficiency depends on the orientation of the transmit dipole captured by $\mathbf{x}$, the orientation of the receive dipole captured by $\mathbf{h}$, and the dielectric properties of the medium captured by $\bar{\mathbf{K}}$. In the following, we will derive the power transfer efficiency that maximizes over all possible orientations of the transmit dipole, and then find the frequency that maximizes this optimal power transfer efficiency for a given receive orientation. Before proceeding to the derivation, we will review the characterization of biological tissue first.

A. Review on Tissue Characterization

At low frequency, the frequency variation of ϵ_r is dominated by the induced current, that is,

$$\epsilon_r(\omega) = \epsilon_{r0} + i\frac{\sigma}{\omega\epsilon_0} \tag{19}$$

where ϵ_{r0} and σ are the static relative permittivity and conductivity respectively. As the operating frequency increases, other loss mechanisms emerge. The dominant one is the dielectric relaxation loss. Debye relaxation model and its variants are popular models for biological media. In this relaxation model, the relative permittivity is expressed as [21]:

$$\epsilon_r(\omega) = \epsilon_\infty + \frac{\epsilon_{r0}-\epsilon_\infty}{1-i\omega\tau} + i\frac{\sigma}{\omega\epsilon_0}. \tag{20}$$

The relaxation phenomenon is model by a first-order equation. Each type of tissue is characterized by 3 parameters: $\epsilon_{r0}, \epsilon_\infty$, and τ. The τ is the relaxation time constant, and its inverse gives the range of frequency where this model is valid. The ϵ_∞ is the relative permittivity at frequencies where $\omega\tau \gg 1$. As we are interested in the efficiency of the power link above 10 MHz, we will use the Debye relaxation model for the frequency range between 10 MHz and 100 GHz in our study. Using muscle as an example, Fig. 3 plots the real part of the relative permittivity and the equivalent conductivity calculated from the imaginary part using parameters from [23].[1] The real part begins to vary with frequency in the GHz-range. From Kramers-Kronig relations [27, Sec. 7.10], the dielectric loss should become significant over the GHz-range. Therefore, we conjecture the existence of an optimal frequency in the GHz-range. Next, we will use the Debye relaxation model to prove our conjecture.

[1]The parameters in [23] are for the 4-term Cole-Cole model which is a variant of the Debye relaxation model. Conversion to the Debye relaxation model is as follows: $\tau = \tau_1, \epsilon_{r0} = \Delta\epsilon_1 + \epsilon_\infty$, and $\sigma = \sum_{n=2}^{4}(\epsilon_0\Delta\epsilon_n)/(\tau_n) + \sigma_s$.

B. Derivation of Optimal Frequency

The orientation of the transmit dipole that maximizes the efficiency in (18) is given by

$$\mathbf{x}_{\text{opt}} = \bar{\mathbf{K}}^{-1}\mathbf{h} \tag{21}$$

and the optimal efficiency is

$$\eta_{\text{opt}} = \frac{|k|^2 A_r^2 \text{Re}\frac{1}{Z_L}}{\omega\epsilon_0 \text{Im}\epsilon_r}\,\mathbf{h}^\dagger\bar{\mathbf{K}}^{-1}\mathbf{h}. \tag{22}$$

Defining $\beta_m = (\psi_{1,m}(-\hat{\mathbf{z}}d))/(|\psi_{1,m}(-\hat{\mathbf{z}}d)|)\cdot\hat{\mathbf{n}}$ for $m = -1, 0, 1$ which are the projections of $\hat{\mathbf{n}}$ onto the directions of the three lowest order multipoles at $-\hat{\mathbf{z}}d$, the optimal efficiency can be written as

$$\eta_{\text{opt}} = \frac{|k|^2 A_r^2 \text{Re}\frac{1}{Z_L}}{\omega\epsilon_0 \text{Im}\epsilon_r}\sum_{m=-1}^{1}|\beta_m|^2\frac{|\boldsymbol{\psi}_{1,m}(-\hat{\mathbf{z}}d)|^2}{\int_{z<-d_1}|\boldsymbol{\xi}_{1,m}(\mathbf{r})|^2\,d\mathbf{r}}. \tag{23}$$

The optimal efficiency is independent of the transmit magnetic moment. From definitions in (10), we obtain

$$\begin{aligned}
&\int_{z<-d_1}|\boldsymbol{\xi}_{1,\pm1}(\mathbf{r})|^2\,d\mathbf{r}\\
&= \frac{e^{-2k_Id_1}}{16|k|^4d_1}\left[9-14k_Id_1+2k_I^2d_1^2-4k_I^3d_1^3\right.\\
&\quad\left.+8|k|^2d_1^2\left(\frac{1}{k_Id_1}-\frac{1}{4}+\frac{k_Id_1}{2}\right)\right]\\
&\quad+\frac{\text{Ei}(-2k_Id_1)}{4|k|^4d_1}\left[|k|^2d_1^2\left(3+2k_I^2d_1^2\right)\right.\\
&\quad\left.-2k_I^2d_1^2\left(3+k_I^2d_1^2\right)\right]
\end{aligned} \tag{24a}$$

$$\begin{aligned}
&\int_{z<-d_1}|\boldsymbol{\xi}_{1,0}(\mathbf{r})|^2\,d\mathbf{r}\\
&= \frac{e^{-2k_Id_1}}{8|k|^4d_1}\left[3-10k_Id_1-2k_I^2d_1^2+4k_I^3d_1^3\right.\\
&\quad\left.+4|k|^2d_1^2\left(\frac{1}{k_Id_1}+\frac{1}{2}-k_Id_1\right)\right]\\
&\quad+\frac{\text{Ei}(-2k_Id_1)}{2|k|^4d_1}\left[|k|^2d_1^2\left(3-2k_I^2d_1^2\right)\right.\\
&\quad\left.-2k_I^2d_1^2\left(3-k_I^2d_1^2\right)\right]
\end{aligned} \tag{24b}$$

and

$$\begin{aligned}
&|\boldsymbol{\psi}_{1,\pm1}(-\hat{\mathbf{z}}d)|^2\\
&= \frac{3e^{-2k_Id}}{4\pi|k|^6d^6}\left[1-|k|^2d^2+|k|^4d^4\right.\\
&\quad\left.+2k_Id\left(1+2k_Id+|k|^2d^2\right)\right]
\end{aligned} \tag{25a}$$

$$\begin{aligned}
&|\boldsymbol{\psi}_{1,0}(-\hat{\mathbf{z}}d)|^2\\
&= \frac{3e^{-2k_Id}}{\pi|k|^6d^6}(1+2k_Id+|k|^2d^2)
\end{aligned} \tag{25b}$$

where $k_I = \text{Im}k$ and $\text{Ei}(\cdot)$ is the exponential integral function.

The relaxation model is valid over the frequency range where $\omega\tau \ll 1$. Over this range, the relative permittivity in (20) is approximately equal to

$$\epsilon_r(\omega) \approx \epsilon_{r0} + i\left(\frac{\sigma}{\omega\epsilon_0} + \omega\tau\Delta\epsilon\right) \tag{26}$$

where $\Delta\epsilon = \epsilon_{r0} - \epsilon_\infty$. This yields

$$k \approx \omega\sqrt{\mu_0\epsilon_0\epsilon_{r0}} + i\frac{\omega}{2}\sqrt{\frac{\mu_0\epsilon_0}{\epsilon_{r0}}}\left(\frac{\sigma}{\omega\epsilon_0} + \omega\tau\Delta\epsilon\right). \tag{27}$$

At high frequency where $1 \ll \omega \ll (1)/(\tau)$, we have the following approximations:

$$|\boldsymbol{\psi}_{1,\pm1}(-\hat{\mathbf{z}}d)|^2 \approx \frac{3e^{-2k_Id}}{4\pi|k|^6d^6}[|k|^4d^4 + |k|^2d^2(2k_Id - 1)] \tag{28a}$$

$$|\boldsymbol{\psi}_{1,0}(-\hat{\mathbf{z}}d)|^2 \approx \frac{3e^{-2k_Id}}{\pi|k|^6d^6}|k|^2d^2. \tag{28b}$$

Assuming d_1 is much smaller than the skin depth, that is, $k_Id_1 \ll 1$

$$\int_{z<-d_1} |\boldsymbol{\xi}_{1,m}(\mathbf{r})|^2\, d\mathbf{r} \approx \frac{1}{2|k|^2k_I}. \tag{29}$$

Putting the above equations together yields

$$\frac{|\boldsymbol{\psi}_{1,\pm1}(-\hat{\mathbf{z}}d)|^2}{\int_{z<-d_1}|\boldsymbol{\xi}_{1,\pm1}(\mathbf{r})|^2\,d\mathbf{r}} \approx \frac{3k_Ie^{-2k_Id}}{2\pi d^4|k|^2} \times (|k|^2d^2 + 2k_Id - 1) \tag{30a}$$

$$\frac{|\boldsymbol{\psi}_{1,0}(-\hat{\mathbf{z}}d)|^2}{\int_{z<-d_1}|\boldsymbol{\xi}_{1,-1}(\mathbf{r})|^2\,d\mathbf{r}} \approx \frac{6k_Ie^{-2k_Id}}{\pi d^4|k|^2}. \tag{30b}$$

Defining $k_{I0} = (\sigma)/(2)\sqrt{(\mu_0)/(\epsilon_0\epsilon_{r0})}$, the optimal efficiency in (23) can then be approximated by

$$\eta_{\text{opt}} \approx \frac{3k_{I0}e^{-2k_{I0}d}A_r^2\text{Re}\frac{1}{Z_L}}{2\pi\sigma d^4}\left[\left(\frac{d^2\epsilon_{r0}}{c^2} + \frac{d\tau\Delta\epsilon}{c\sqrt{\epsilon_{r0}}}\right)\cdot(|\beta_{-1}|^2 + |\beta_1|^2)\omega^2 + 4|\beta_0|^2 - |\beta_{-1}|^2 - |\beta_1|^2 + 2k_{I0}d(|\beta_{-1}|^2 + |\beta_1|^2)\right]e^{-d\tau\Delta\epsilon/c\sqrt{\epsilon_{r0}}\omega^2}. \tag{31}$$

It is maximized as in (32), shown at the bottom of the page. Gabriel *et al.* have experimentally characterized the dielectric properties of 17 kinds of biological tissue [23]. In general, $(d^2\epsilon_{r0})/(c^2) \gg (d\tau\Delta\epsilon)/(c\sqrt{\epsilon_{r0}})$. Therefore, we have

$$\omega_{\text{opt}} \approx \sqrt{\frac{c\sqrt{\epsilon_{r0}}}{d\tau\Delta\epsilon}}. \tag{33}$$

The optimal frequency is approximately inversely proportional to the square root of transmit-receive separation.

TABLE I
APPROXIMATE OPTIMAL FREQUENCY FOR 17 DIFFERENT TYPES OF BIOLOGICAL TISSUE, ASSUMING $d = 1$ cm

Type of tissue	Approximate f_{opt} (GHz)
Blood	3.54
Bone (cancellous)	3.80
Bone (cortical)	4.50
Brain (grey matter)	3.85
Brain (white matter)	4.23
Fat (infiltrated)	6.00
Fat (not infiltrated)	8.64
Heart	3.75
Kidney	3.81
Lens cortex	3.93
Liver	3.80
Lung	4.90
Muscle	3.93
Skin (dry)	4.44
Skin (wet)	4.01
Spleen	3.79
Tendon	3.17

At the optimal frequency, the approximated efficiency in (31) is lower-bounded by

$$\begin{aligned}\eta_{\text{opt}} &> \frac{3k_{I0}e^{-2k_{I0}d}A_r^2\text{Re}\frac{1}{Z_L}}{2\pi\sigma d^4}\left(\frac{d^2\epsilon_{r0}}{c^2} + \frac{d\tau\Delta\epsilon}{c\sqrt{\epsilon_{r0}}}\right)\\ &\quad\cdot(|\beta_{-1}|^2 + |\beta_1|^2)\frac{c\sqrt{\epsilon_{r0}}}{d\tau\Delta\epsilon}e^{-1}\\ &\approx \frac{3\sqrt{\mu_0/\epsilon_0}\epsilon_{r0}e^{-2k_{I0}d-1}A_r^2\text{Re}\frac{1}{Z_L}}{4\pi c\tau\Delta\epsilon d^3}(|\beta_{-1}|^2 + |\beta_1|^2)\\ &\propto \frac{1}{d^3}.\end{aligned} \tag{34}$$

It is approximately inversely proportional to the cube of the transmit-receive separation. In the far field, the power gain follows the inverse square law; that is, it is inversely proportional to the square of the transmit-receive separation. In the near field, the power gain is inversely proportional to the 6th power of the transmit-receive separation. Now, the optimal efficiency is somewhere in between the far field and the near field.

C. Numerical Examples

Based on the measured data in [23], Table I lists the approximated optimal frequencies for 17 different kinds of tissue assuming $d = 1$ cm. All approximated optimal frequencies are in the GHz-range. They are above 1 GHz even for $d = 10$ cm.

As muscle is the most widely reported tissue, let us take muscle as an example. We consider a receive dipole tilted 45° with respect to the z-axis; that is, $\beta_{-1} = \beta_1 = 1/2, \beta_0 = 1/\sqrt{2}$. The area of the receive dipole is $(2\text{ mm})^2$. We first compute the efficiency given in (23) that optimizes the orientation of the transmit dipole for the given β_m's, over the frequency range between 1 MHz and 10 GHz. Then, we find the efficiency that

$$\omega_{\text{opt}} = \sqrt{\frac{c\sqrt{\epsilon_{r0}}}{d\tau\Delta\epsilon} - \frac{4|\beta_0|^2 - |\beta_{-1}|^2 - |\beta_1|^2 + 2k_{I0}d\,(|\beta_{-1}|^2 + |\beta_1|^2)}{\left(\frac{d^2\epsilon_{r0}}{c^2} + \frac{d\tau\Delta\epsilon}{c\sqrt{\epsilon_{r0}}}\right)(|\beta_{-1}|^2 + |\beta_1|^2)}}. \tag{32}$$

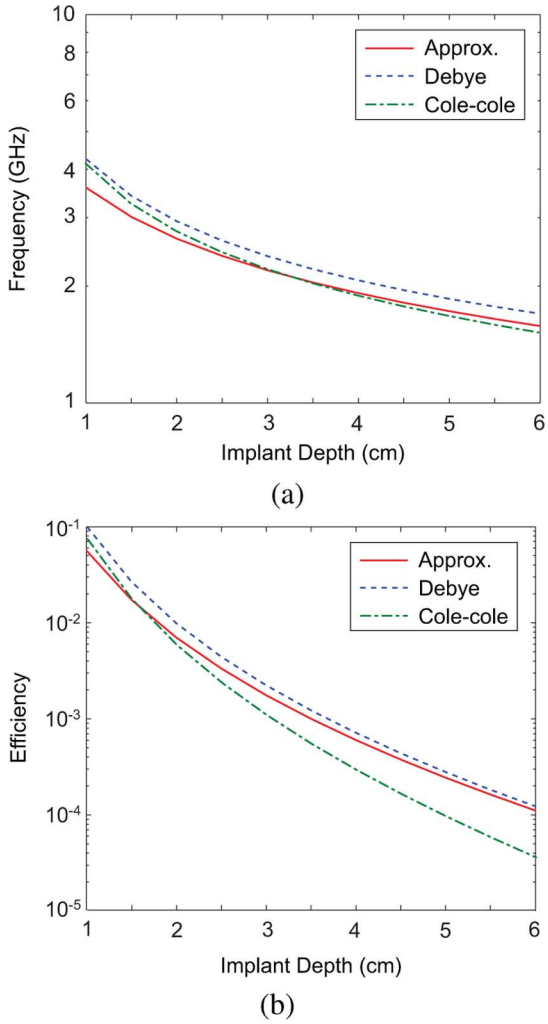

Fig. 4. Dipole source in homogeneous medium—(a) optimal frequency with $d_1 = 2$ mm and receive dipole tilted 45°; and (b) optimal efficiency with $A_r = (2\text{ mm})^2$ and $Z_L = 1\ \Omega$.

is maximized across this frequency range for different implant depth, $d - d_1$, and compare them with the approximations in (33). Fig. 4(a) shows these curves. The approximated and the exact optimal frequencies based on the Debye relaxation model are very close. Hence, the formula in (33) is a good approximation. We also plot the efficiency at the optimal frequency and compare it with the approximation in (34). The two curves are shown in Fig. 4(b). The approximation shows good matches as well.

As a number of commercial electromagnetic field solvers that include human body model use the 4-term Cole-Cole model which is a variant of the Debye relaxation model. We also compute the exact optimal frequencies based on the Cole-Cole model. For reference, Fig. 3 compares the dielectric properties of muscle between the two relaxation models. Fig. 4 shows that the two models yield similar results.

D. Variation of Penetration Depth With Frequency

Now, we attempt to understand the reason behind the popular use of low-frequency carrier in wireless power transmission for implantable systems. In (19), the low-frequency relative permittivity captures the effect of displacement current and induced-current loss. When the frequency is low enough, the imaginary component dominates, that is, the induce current is substantial whereas the displacement current is negligible. The wavenumber can be approximated by

$$k = \sqrt{\frac{\omega\mu_0\sigma}{2}}(1+i). \tag{35}$$

The skin depth $\delta_{\text{quasi static}}$ is given by the inverse of the imaginary part of k

$$\delta_{\text{quasi static}} = \sqrt{\frac{2}{\omega\mu_0\sigma}} \propto \frac{1}{\sqrt{\omega}} \tag{36}$$

It is inversely proportional to the square root of frequency. According to this low-frequency model, the efficiency decreases exponentially with $\sqrt{\omega}$. It is worse to operate at higher frequencies than at DC. However, this low-frequency model cannot be used to conclude the behavior at higher frequencies. At high frequency, the imaginary part should be approximated by the expression in (27). The skin depth $\delta_{\text{full wave}}$ is approximated by

$$\delta_{\text{full wave}} = \frac{2}{\sigma + \omega^2\tau\epsilon_0\Delta\epsilon}\sqrt{\frac{\epsilon_0\epsilon_{r0}}{\mu_0}}. \tag{37}$$

Depending on ω, the skin depth is invariant with frequency when $\sigma \gg \omega^2\tau\epsilon_0\Delta\epsilon$, and it is inversely proportional to the square of frequency when $\sigma \ll \omega^2\tau\epsilon_0\Delta\epsilon$. This transition introduces the optimal frequency in the GHz-range.

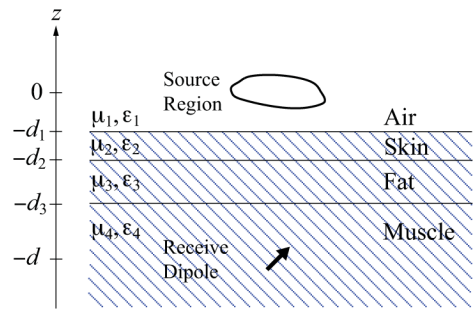

Fig. 5. A planarly layered medium.

IV. Optimal Frequency in Planarly Layered Body Model

The analyses in homogeneous medium reveal that the effect of tissue absorption on the power transfer efficiency is not as worse as we used to believe. Higher efficiency can be achieved by operating at higher frequency until reaching the optimal frequency. In this section, we include the air-tissue interface and study its effect on the optimal frequency. We model human body as a planarly layered medium, as illustrated in Fig. 5. The analysis can be extended to other inhomogeneous media such as spherically layered medium and cylindrically layered medium which may provide a better model for certain part of the body.

A. Dipole Source

For small source region, the lowest order multipole fields in (12) correspond to fields emanated from the

three orthogonal magnetic dipoles. More specifically, $1/\sqrt{2}\boldsymbol{\psi}_{1,-1}(\mathbf{r})-1/\sqrt{2}\boldsymbol{\psi}_{1,1}(\mathbf{r}), 1/\sqrt{2}\boldsymbol{\psi}_{1,-1}(\mathbf{r})+1/\sqrt{2}\boldsymbol{\psi}_{1,1}(\mathbf{r})$, and $\boldsymbol{\psi}_{1,0}(\mathbf{r})$ give the magnetic fields due to magnetic dipole pointing in the x, y, and z directions respectively. In a homogeneous medium, they can be obtained from each other by rotation transformations. In a layered medium, we need to distinguish between horizontal magnetic dipole (HMD) and vertical magnetic dipole (VMD). The electromagnetic fields due to dipoles pointing in the x and y directions can be obtained from the HMD while those due to a dipole pointing in the z direction can be obtained from the VMD.

For convenience, we use the same symbols as in the homogeneous medium. We denote the magnetic fields due to the three lowest order multipoles by $\boldsymbol{\psi}_x(\mathbf{r}), \boldsymbol{\psi}_y(\mathbf{r})$, and $\boldsymbol{\psi}_z(\mathbf{r})$, and their electric field counterparts by $\boldsymbol{\xi}_x(\mathbf{r}), \boldsymbol{\xi}_y(\mathbf{r})$, and $\boldsymbol{\xi}_z(\mathbf{r})$. The electromagnetic fields are then given by

$$\mathbf{H}(\mathbf{r}) = \frac{1}{4\pi}[\alpha_x\boldsymbol{\psi}_x(\mathbf{r}) + \alpha_y\boldsymbol{\psi}_y(\mathbf{r}) + \alpha_z\boldsymbol{\psi}_z(\mathbf{r})] \quad (38a)$$

$$\mathbf{E}(\mathbf{r}) = -\frac{\omega\mu_0}{4\pi}[\alpha_x\boldsymbol{\xi}_x(\mathbf{r}) + \alpha_y\boldsymbol{\xi}_y(\mathbf{r}) + \alpha_z\boldsymbol{\xi}_z(\mathbf{r})]. \quad (38b)$$

Now, the direction of $(\alpha_x, \alpha_y, \alpha_z)$ gives the orientation of the transmit dipole and its magnitude gives the transmit magnetic moment. As most advanced electromagnetic textbooks do not include the complete set of expressions for $\boldsymbol{\psi}_m(\mathbf{r})$'s and $\boldsymbol{\xi}_m(\mathbf{r})$'s, we summarize it in Appendix A. With similar definitions as in (16), we obtain the matrix form for the power transfer efficiency same as in (18). By symmetry, $\bar{\mathbf{K}}$ is also a diagonal matrix. Therefore, the optimal efficiency is similar to (23) and is given by

$$\eta_{\text{opt}} = \frac{A_r^2 \text{Re}\frac{1}{Z_L}}{\omega\epsilon_0} \sum_{m\in\{x,y,z\}} \frac{|\beta_m|^2\,|\boldsymbol{\psi}_m(-\hat{\mathbf{z}}d)|^2}{\int_{z<-d_1} \text{Im}\epsilon_r(\mathbf{r})|\boldsymbol{\xi}_m(\mathbf{r})|^2\,d\mathbf{r}}. \quad (39)$$

For given d and β_m's, the frequency that maximizes this efficiency gives the optimal frequency. Unlike in the homogeneous medium, closed-form expressions for the terms inside the summation are not feasible. Therefore, we cannot obtain a closed form expression for the optimal frequency.

We numerically compute the optimal frequency for two cases. In the first case, it is a halfspace with air in medium 1 and muscle in medium 2. In the second case, we consider an air-skin-fat-muscle multi-layered medium. In both cases, we use the measured data in [23] to model the dielectric dispersion of biological tissues. To accelerate the computation of the Sommerfeld integrals involved in the expressions for $\boldsymbol{\psi}_m(\mathbf{r})$'s and $\boldsymbol{\xi}_m(\mathbf{r})$'s, we follow [28] to deform the integration path. Furthermore, as the integrals involve Bessel functions which are oscillatory, we partition the revised integration path into sub-paths with exponentially increasing length, and perform the integration over these sub-paths.

Fig. 6(a) plots the optimal frequency versus the implant depth, $d-d_1$. The transmit dipole is 1 cm above the tissue interface and the receive dipole is tilted 45° with respect to the z axis. In the air-skin-fat-muscle multi-layered medium, the thickness of skin is 2 mm and the thickness of fat is 5 mm. We also include the curve from the last section for homogeneous medium (denote by "muscle" in the figure) where the transmit dipole is 2 mm

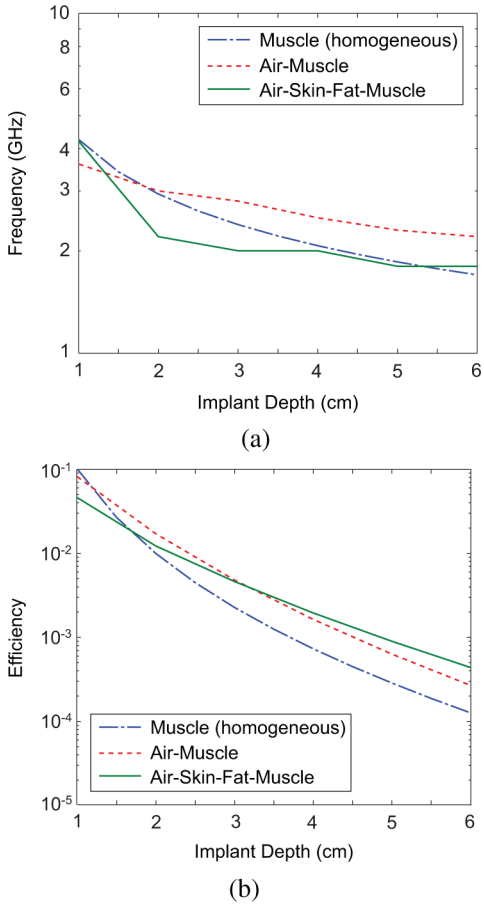

Fig. 6. Dipole source in planarly layered medium—(a) optimal frequency with $(d_1, d_2, d_3) = (1\text{ cm}, 1.2\text{ cm}, 1.7\text{ cm})$ and receive dipole tilted 45°; and (b) optimal efficiency with $A_r = (2\text{ mm})^2$ and $Z_L = 1\ \Omega$.

above the interface. All optimal frequencies are above 1 GHz. They vary with different thickness of tissues. In typical tissue compositions, they are in the GHz-range. Fig. 6(b) plots the efficiency at the optimal frequency versus the implant depth. The efficiency is not very sensitive to the variation of tissue composition. Its variation with the implant depth remains approximately inversely proportional to d^3.

B. Uniform Source Region

The analysis based on dipole source is carried over from homogeneous medium to layered medium. Now we consider a finite dimensional source region. Assume that we could implement a sheet of fully controlled source elements in the region. If all source elements have identical current and point in the z direction, the source current density becomes

$$\mathbf{M}_{tx}(\mathbf{r}) = -\hat{\mathbf{z}}i\omega\mu_0 I_t A_t \delta(z), \quad |x|, |y| \le \sqrt{A_t}/2. \quad (40)$$

This is equivalent to a square current loop of area A_t with uniform current I_t. The electromagnetic fields can be obtained from those due to VMD and are given by

$$\mathbf{H}(\mathbf{r}) = \frac{I_t A_t}{4\pi} \int_{|x'|,|y'|<\sqrt{A_t}/2, z'=0} \boldsymbol{\psi}_z(\mathbf{r}-\mathbf{r}')\,d\mathbf{r}' \quad (41a)$$

$$\mathbf{E}(\mathbf{r}) = -\frac{\omega\mu_0 I_t A_t}{4\pi} \int_{|x'|,|y'|<\sqrt{A_t}/2, z'=0} \boldsymbol{\xi}_z(\mathbf{r}-\mathbf{r}')\,d\mathbf{r}'. \quad (41b)$$

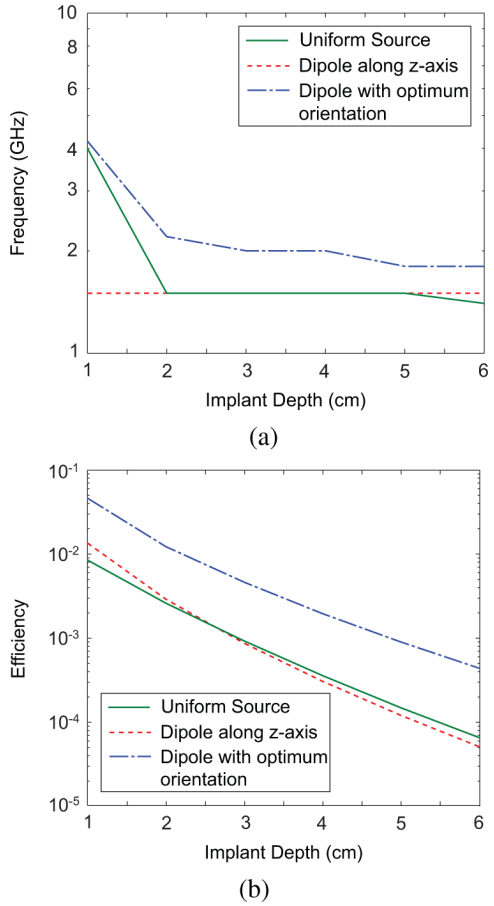

Fig. 7. Uniform source in planarly layered medium—(a) optimal frequency with $(d_1, d_2, d_3) =$ (1 cm, 1.2 cm, 1.7 cm), receive dipole tilted 45°, and $A_t = (2\text{ cm})^2$; and (b) optimal efficiency with $A_r =$ (2 mm)^2 and $Z_L = 1\Omega$.

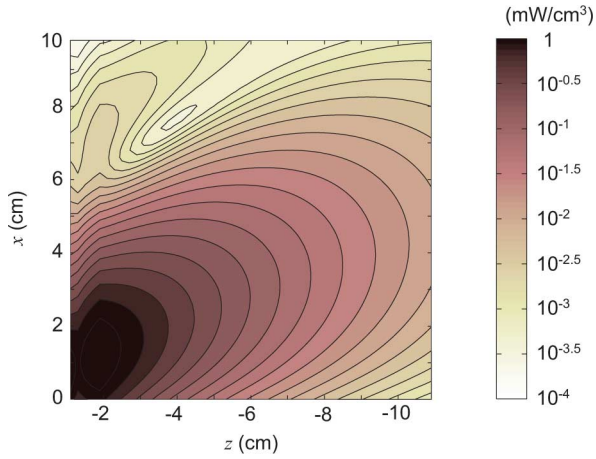

Fig. 8. Local SAR distribution at 1 GHz for $(d_1, d_2, d_3) =$ (1 cm, 1.2 cm, 1.7 cm) and $A_t =$ (2 cm)^2.

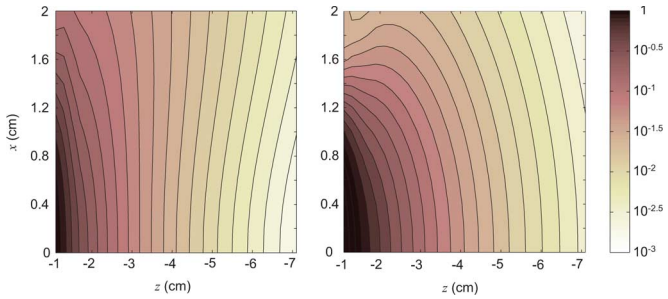

Fig. 9. Received power distribution at 1 GHz for $A_t =$ (2 cm)^2, $A_r =$ (2 mm)^2, $Z_L = 5.6\ \Omega$, and receive dipole (left) tilted 45° and (right) pointing in the z direction.

The frequency that maximizes the efficiency defined in (7), is the optimal frequency. When dipole sources are used, the efficiency does not depend on the area of the transmit dipole. Here, the efficiency will depend on the area of the transmit source.

Fig. 7(a) plots the optimal frequency versus the implant depth for $A_t = (2\text{ cm})^2$. All optimal frequencies are above 1 GHz. Fig. 7(b) plots the efficiency at the optimal frequency versus the implant depth (the solid line). The efficiency is about 5 dB worse than that obtained from the dipole-source analysis. This is because the orientation of the transmit dipole is optimized for the given orientation of the receive dipole. As all the source elements in the transmit region are pointing in the z direction, we compare the efficiency with that due to a transmit dipole pointing in the z direction. The two curves match well. This numerical example reveals that dipole-source analysis is a good approximation, and much higher efficiency is possible if transmit sources can orient freely.

C. Local SAR Calculations

With a finite dimensional source, we can investigate the distribution of heat absorption inside tissue. From which, we can obtain the transmit magnetic moment that satisfies the safety guidelines. As the transmit source is close to the tissue, we adopt the safety guidelines for specific absorption rate (SAR). In the IEEE guideline, the SAR limits are 1.6 W/kg for any 1 g of tissue and 4 W/kg for any 10 g of tissue. In the ICNIRP guideline, the SAR limit is 4 W/kg for any 10 g of tissue in hands, wrists, feet, and ankles, and 2 W/kg for any 10 g of other tissue. In general, 1 g of tissue approximately occupies 1 cm^3 and 10 g of tissue occupies 2.15 cm^3. That is, the tissue absorption should not exceed 1.6 mW in 1 cm^3 and 20 mW to 40 mW in 2.15 cm^3.

We consider a square loop of width 2 cm at a distance 1 cm above the air-tissue interface and an air-skin-fat-muscle multilayered medium with $(d_1, d_2, d_3) =$ (1 cm, 1.2 cm, 1.7 cm). We first assume $I_t A_t$ equal to 1 Am^2 and compute the SAR distribution. Then, we scale the SAR distribution by a factor such that the maximum value of the scaled distribution equals to 1.6 mW/cm^3. This scaling factor also gives the transmit current which is 280 mA. Fig. 8 plots the SAR distribution at 1 GHz after scaling. The corresponding received power distributions are plotted in Fig. 9 for two receive dipole orientations. At an implant depth of 2 cm ($z = -3$ cm), the received power is 67 μW for a dipole tilted 45° and 150 μW for a dipole pointing in the z direction. If the less stringent SAR limit is used, the received power will be increased by approximately 10 times. As a result, sub-mW to mW of power can be safely delivered to a mm-sized receive antenna from a cm-sized transmit antenna with a separation of a few cm at carrier frequency of 1 GHz.

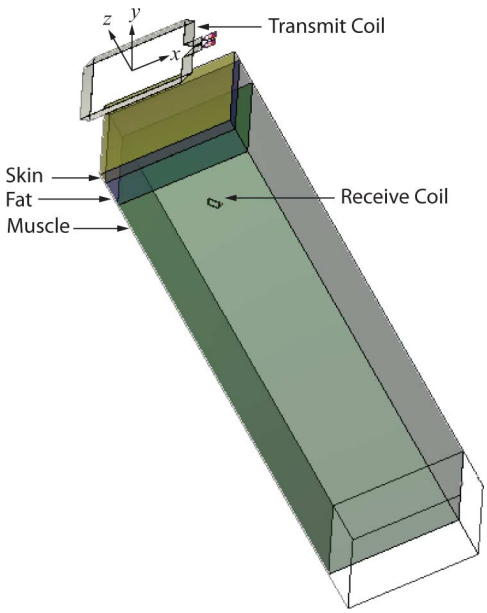

Fig. 10. 3D view of the transmit coil, the receive coil, and the tissue model in IE3D.

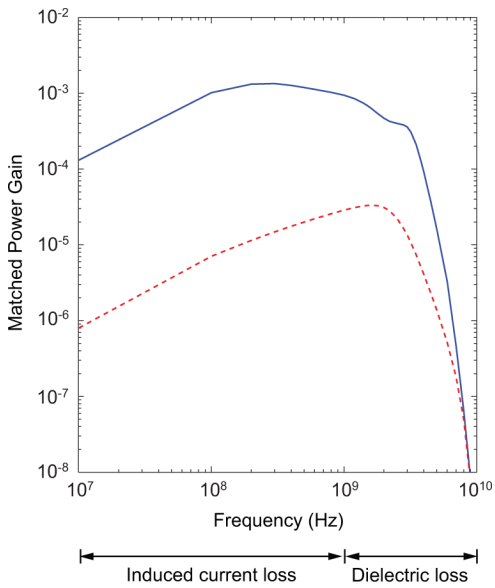

Fig. 11. Simulated matched power gain versus frequency for transmit coil of width (solid line) 2 cm and (dotted line) 2 mm, and $d - d_1 = 2$ cm.

V. Optimal Frequency With Conjugate Matching at Receiver

The received power depends on the load impedance Z_L. In the inductively coupled link, the load impedance is chosen to achieve a given output voltage. Various tuning configurations—series vs. shunt tuning—are then chosen to maximize the power transfer efficiency. Shunt tuning at receiver and series tuning at transmitter is commonly used. At 1 GHz or above, the mutual impedance between the transmit and the receive antennas is no longer purely imaginary as in the inductive link. We should use a different approach and model the power link as a two-port network. As our objective is to maximize the power transfer efficiency, we should perform simultaneously conjugate matching at both transmitter and receiver. The output voltage requirement is then fulfilled by the choice of different forms of matching network. As a result, the load impedance Z_L in the definition of P_r in (6) is related to the self-impedance of the receive antenna. At conjugate matching, the total impedance of port 2 is approximately equal to 2 times the real part of the self-impedance and half of the power absorbed by port 2 goes to the load. Therefore, the load impedance Z_L in the definition of P_r can be chosen to be 4 times the real part of the self-impedance. In the last section, we choose $Z_L = 5.6\,\Omega$ which is 4 times the resistance of a 2-mm side square copper loop with a trace width of 0.20 mm and trace thickness of 0.04 mm.

As the self-impedance of the receive antenna changes with frequency, the optimal choice of Z_L changes with frequency as well. To understand the effect of load impedance on the optimal frequency, we perform electromagnetic simulations. We use Zeland IE3D full-wave electromagnetic field solver [24] to obtain the S-parameters for the 2-port system in Fig. 10. The tissue model is the air-skin-fat-muscle planarly layered structure with same thicknesses as in previous examples. The frequency dependence of the tissue dielectric properties is imported to the simulator according to the dielectric model in [23]. Both transmit and receive coils are single-turn. The transmit coil is a 2-cm side square copper loop with a trace width of 2.00 mm and trace thickness of 0.04 mm. The receive coil is a 2-mm side square copper loop with a trace width of 0.20 mm and trace thickness of 0.04 mm. The transmit coil is in parallel with the tissue interface and is 1 cm above it, while the receive coil is tilted 45° and is 2 cm below the interface. Both coils are axially aligned.

Fig. 11 plots the variation of matched power gain with frequency. The loss in the matched power gain includes not only tissue absorption but also ohmic loss in both coils and radiation loss from the transmit coil. At low frequency, the ohmic loss dominates but its rate of increase with frequency is less than that of the received power. As a result, the power gain increases with frequency. The rate of increase reduces when loss from induced current dominates. Finally, it decreases steeply with frequency when dielectric loss dominates.

The optimal frequency for the 2-cm side transmit coil shifts to the sub-GHz range due to radiation loss. The wavelength at 1 GHz is about 4 cm and therefore, radiation loss plays a role in the sub-GHz range. When a smaller transmit coil is used (dotted line in Fig. 11), the optimal frequency remains in the GHz-range. This suggests that we should consider using an antenna array in the GHz-range. The array pattern can be controlled to maximize the received power while minimizing the total tissue absorption and local SAR. Similar technique is applied to hyperthermia operating in the GHz-range. In hyperthermia, there is an optimal frequency when an array of applicators is used, but such an optimal frequency does not exist for a single applicator. Here, power delivery to an implant has an optimal frequency even for a single transmit antenna.

VI. Conclusion

Wireless power transmission into biological tissue usually operates below 10 MHz, and quasi-static approximation and

transformer model are commonly used in the analysis of the power link. In this paper, we perform full-wave analysis and model the power link as a generalized two-port network. The optimal frequency is in the GHz-range when the dimension of the transmit antenna is much smaller than a wavelength. It shifts to the sub-GHz range when the dimension is comparable to a wavelength. This suggests that we should consider using an antenna array to increase the power transfer efficiency, similar to focused hyperthermia. As the optimal frequency is about 2 order of magnitude higher than what is used today, dramatic receiver miniaturization is feasible. In addition, operating at higher frequency desensitizes the effect of receive coil orientation as now it is no longer in the near field of the transmitter. To exploit these advantages require new models and new circuit design techniques which can be the directions for future research in this area.

APPENDIX

A. Expressions for Field Components in (38a)–(38b)

The $\boldsymbol{\psi}_i(\mathbf{r})$'s in Cartesian coordinates can be written in terms of the TE and TM components

$$\begin{aligned}
\boldsymbol{\psi}_{xx}(\mathbf{r}) &= \left(\psi^{te}_{hmd,\rho}(\mathbf{r}) + \psi^{tm}_{hmd,\rho}(\mathbf{r})\right)\cos^2\phi \\
&\quad - \left(\psi^{te}_{hmd,\phi}(\mathbf{r}) + \psi^{tm}_{hmd,\phi}(\mathbf{r})\right)\sin^2\phi \\
\boldsymbol{\psi}_{xy}(\mathbf{r}) &= \left(\psi^{te}_{hmd,\rho}(\mathbf{r}) + \psi^{tm}_{hmd,\rho}(\mathbf{r})\right)\cos\phi\sin\phi \\
&\quad + \left(\psi^{te}_{hmd,\phi}(\mathbf{r}) + \psi^{tm}_{hmd,\phi}(\mathbf{r})\right)\cos\phi\sin\phi \\
\boldsymbol{\psi}_{xz}(\mathbf{r}) &= \psi^{te}_{hmd,z}(\mathbf{r})\cos\phi \\
\boldsymbol{\psi}_{yx}(\mathbf{r}) &= \left(\psi^{te}_{hmd,\rho}(\mathbf{r}) + \psi^{tm}_{hmd,\rho}(\mathbf{r})\right)\cos\phi\sin\phi \\
&\quad + \left(\psi^{te}_{hmd,\phi}(\mathbf{r}) + \psi^{tm}_{hmd,\phi}(\mathbf{r})\right)\cos\phi\sin\phi \\
\boldsymbol{\psi}_{yy}(\mathbf{r}) &= \left(\psi^{te}_{hmd,\rho}(\mathbf{r}) + \psi^{tm}_{hmd,\rho}(\mathbf{r})\right)\sin^2\phi \\
&\quad - \left(\psi^{te}_{hmd,\phi}(\mathbf{r}) + \psi^{tm}_{hmd,\phi}(\mathbf{r})\right)\cos^2\phi \\
\boldsymbol{\psi}_{yz}(\mathbf{r}) &= \psi^{te}_{hmd,z}(\mathbf{r})\sin\phi \\
\boldsymbol{\psi}_{zx}(\mathbf{r}) &= \psi^{te}_{vmd,\rho}(\mathbf{r})\cos\phi \\
\boldsymbol{\psi}_{zy}(\mathbf{r}) &= \psi^{te}_{vmd,\rho}(\mathbf{r})\sin\phi \\
\boldsymbol{\psi}_{zz}(\mathbf{r}) &= \psi^{te}_{vmd,z}(\mathbf{r}).
\end{aligned}$$

Defining $k_n = \omega(\mu_0\epsilon_0\epsilon_n)^{1/2}$ and $k_{nz} = (k_n^2 - k_\rho^2)^{1/2}$, the TE and TM components for $\mathbf{r}$ in the nth layer are given by

$$\begin{aligned}
&\psi^{te}_{hmd,\rho}(\mathbf{r}) \\
&= i\int_0^\infty k_\rho k_{nz} J_1'(k_\rho\rho)A_n\left[e^{-ik_{nz}z} - \tilde{R}^{te}_{n,n+1}e^{ik_{nz}(z+2d_n)}\right]dk_\rho \\
&\psi^{tm}_{hmd,\rho}(\mathbf{r}) \\
&= \frac{ik_1^2}{\rho}\int_0^\infty \frac{1}{k_{1z}}J_1(k_\rho\rho)A_n \\
&\quad\cdot\left[e^{-ik_{nz}z} + \tilde{R}^{tm}_{n,n+1}e^{ik_{nz}(z+2d_n)}\right]dk_\rho \\
&\psi^{te}_{hmd,\phi}(\mathbf{r}) \\
&= -\frac{i}{\rho}\int_0^\infty k_{nz}J_1(k_\rho\rho)A_n\left[e^{-ik_{nz}z} - \tilde{R}^{te}_{n,n+1}e^{ik_{nz}(z+2d_n)}\right]dk_\rho \\
&\psi^{tm}_{hmd,\phi}(\mathbf{r}) \\
&= -ik_1^2\int_0^\infty \frac{k_\rho}{k_{1z}}J_1'(k_\rho\rho)A_n \\
&\quad\cdot\left[e^{-ik_{nz}z} + \tilde{R}^{tm}_{n,n+1}e^{ik_{nz}(z+2d_n)}\right]dk_\rho \\
&\psi^{te}_{hmd,z}(\mathbf{r}) \\
&= -\int_0^\infty k_\rho^2 J_1(k_\rho\rho)A_n\left[e^{-ik_{nz}z} + \tilde{R}^{te}_{n,n+1}e^{ik_{nz}(z+2d_n)}\right]dk_\rho \\
&\psi^{te}_{vmd,\rho}(\mathbf{r}) \\
&= -\int_0^\infty \frac{k_\rho^2 k_{nz}}{k_{1z}}J_1(k_\rho\rho)A_n \\
&\quad\cdot\left[e^{-ik_{nz}z} - \tilde{R}^{te}_{n,n+1}e^{ik_{nz}(z+2d_n)}\right]dk_\rho \\
&\psi^{te}_{vmd,z}(\mathbf{r}) \\
&= i\int_0^\infty \frac{k_\rho^3}{k_{1z}}J_0(k_\rho\rho)A_n\left[e^{-ik_{nz}z} + \tilde{R}^{te}_{n,n+1}e^{ik_{nz}(z+2d_n)}\right]dk_\rho.
\end{aligned}$$

Similarly, the $\boldsymbol{\xi}_i(\mathbf{r})$'s in Cartesian coordinates can be written as

$$\begin{aligned}
\boldsymbol{\xi}_{xx}(\mathbf{r}) &= \left(\xi^{te}_{hmd,\rho}(\mathbf{r}) + \xi^{tm}_{hmd,\rho}(\mathbf{r})\right)\cos\phi\sin\phi \\
&\quad - \left(\xi^{te}_{hmd,\phi}(\mathbf{r}) + \xi^{tm}_{hmd,\phi}(\mathbf{r})\right)\cos\phi\sin\phi \\
\boldsymbol{\xi}_{xy}(\mathbf{r}) &= \left(\xi^{te}_{hmd,\rho}(\mathbf{r}) + \xi^{tm}_{hmd,\rho}(\mathbf{r})\right)\sin^2\phi \\
&\quad + \left(\xi^{te}_{hmd,\phi}(\mathbf{r}) + \xi^{tm}_{hmd,\phi}(\mathbf{r})\right)\cos^2\phi \\
\boldsymbol{\xi}_{xz}(\mathbf{r}) &= \psi^{tm}_{hmd,z}(\mathbf{r})\sin\phi \\
\boldsymbol{\xi}_{yx}(\mathbf{r}) &= -\left(\xi^{te}_{hmd,\rho}(\mathbf{r}) + \xi^{tm}_{hmd,\rho}(\mathbf{r})\right)\cos^2\phi \\
&\quad - \left(\xi^{te}_{hmd,\phi}(\mathbf{r}) + \xi^{tm}_{hmd,\phi}(\mathbf{r})\right)\sin^2\phi \\
\boldsymbol{\xi}_{yy}(\mathbf{r}) &= -\left(\xi^{te}_{hmd,\rho}(\mathbf{r}) + \xi^{tm}_{hmd,\rho}(\mathbf{r})\right)\cos\phi\sin\phi \\
&\quad + \left(\xi^{te}_{hmd,\phi}(\mathbf{r}) + \xi^{tm}_{hmd,\phi}(\mathbf{r})\right)\cos\phi\sin\phi \\
\boldsymbol{\xi}_{yz}(\mathbf{r}) &= -\xi^{tm}_{hmd,z}(\mathbf{r})\cos\phi \\
\boldsymbol{\xi}_{zx}(\mathbf{r}) &= -\xi^{te}_{vmd,\phi}(\mathbf{r})\sin\phi \\
\boldsymbol{\xi}_{zy}(\mathbf{r}) &= \xi^{te}_{vmd,\phi}(\mathbf{r})\cos\phi \\
\boldsymbol{\xi}_{zz}(\mathbf{r}) &= 0.
\end{aligned}$$

The corresponding TE and TM components are given by

$$\begin{aligned}
&\xi^{te}_{hmd,\rho}(\mathbf{r}) \\
&= \frac{i}{\rho}\int_0^\infty J_1(k_\rho\rho)A_n\left[e^{-ik_{nz}z} + \tilde{R}^{te}_{n,n+1}e^{ik_{nz}(z+2d_n)}\right]dk_\rho \\
&\xi^{tm}_{hmd,\rho}(\mathbf{r}) \\
&= \frac{i\epsilon_1}{\epsilon_n}\int_0^\infty \frac{k_\rho k_{nz}}{k_{1z}}J_1'(k_\rho\rho)A_n \\
&\quad\cdot\left[e^{-ik_{nz}z} - \tilde{R}^{tm}_{n,n+1}e^{ik_{nz}(z+2d_n)}\right]dk_\rho \\
&\xi^{te}_{hmd,\phi}(\mathbf{r}) \\
&= i\int_0^\infty k_\rho J_1'(k_\rho\rho)A_n\left[e^{-ik_{nz}z} + \tilde{R}^{te}_{n,n+1}e^{ik_{nz}(z+2d_n)}\right]dk_\rho \\
&\xi^{tm}_{hmd,\phi}(\mathbf{r}) \\
&= \frac{i\epsilon_1}{\rho\epsilon_n}\int_0^\infty \frac{k_{nz}}{k_{1z}}J_1(k_\rho\rho)A_n \\
&\quad\cdot\left[e^{-ik_{nz}z} - \tilde{R}^{tm}_{n,n+1}e^{ik_{nz}(z+2d_n)}\right]dk_\rho \\
&\xi^{tm}_{hmd,z}(\mathbf{r})
\end{aligned}$$

$$= -\frac{\epsilon_1}{\epsilon_n}\int_0^\infty \frac{k_\rho^2}{k_{1z}} J_1(k_\rho\rho) A_n \cdot \left[e^{-ik_{nz}z} + \tilde{R}^{tm}_{n,n+1} e^{ik_{nz}(z+2d_n)}\right] dk_\rho$$

$$\xi^{te}_{vmd,\phi}(\mathbf{r}) = -\int_0^\infty \frac{k_\rho^2}{k_{1z}} J_1(k_\rho\rho) A_n \left[e^{-ik_{nz}z} + \tilde{R}^{te}_{n,n+1} e^{ik_{nz}(z+2d_n)}\right] dk_\rho.$$

In the above expressions, the generalized reflection coefficients $\tilde{R}_{n,n+1}$ and amplitudes A_n can be obtained from the following recursive relations:

$$\tilde{R}_{n,n+1} = \frac{R_{n,n+1} + \tilde{R}_{n+1,n+2} e^{i2k_{n+1,z}(d_{n+1}-d_n)}}{1 + R_{n,n+1}\tilde{R}_{n+1,n+2} * e^{i2k_{n+1,z}(d_{n+1}-d_n)}}$$

$$A_n = \frac{(1+R_{n-1,n})A_{n-1} e^{i(k_{n-1,z}-k_{nz})d_{n-1}}}{1 + R_{n-1,n}\tilde{R}_{n,n+1} e^{i2k_{nz}(d_n - d_{n-1})}}$$

where the reflection coefficients for the TE and TM components are

$$R^{te}_{n,n+1} = \frac{k_{nz} - k_{n+1,z}}{k_{nz} + k_{n+1,z}}$$

$$R^{tm}_{n,n+1} = \frac{\epsilon_{n+1}k_{nz} - \epsilon_n k_{n+1,z}}{\epsilon_{n+1}k_{nz} + \epsilon_n k_{n+1,z}}.$$

ACKNOWLEDGMENT

The authors would like to thank Prof. W.-C. Chew for the useful discussions and valuable comments.

REFERENCES

[1] J. C. Schuder, H. E. Stephenson Jr., and J. F. Townsend, "High-level electromagnetic energy transfer through a closed chest wall," *IRE Int. Conv. Record*, vol. 9, pp. 119–126, 1961.

[2] J. C. Schuder, J. H. Gold, H. Stoeckle, and J. A. Holland, "The relationship between the electric field in a semi-infinite conductive region and the power input to a circular coil on or above the surface," *Med. Biol. Eng.*, vol. 14, no. 2, pp. 227–234, Mar. 1976.

[3] F. C. Flack, E. D. James, and D. M. Schlapp, "Mutual inductance of air-cored coils: Effect on design of radio-frequency coupled implants," *Med. Biol. Eng.*, vol. 9, no. 2, pp. 79–85, Mar. 1971.

[4] D. C. Galbraith, "An Implantable Multichannel Neural Stimulator," Ph.D. dissertation, Stanford University, , Dec. 1984.

[5] W. J. Heetderks, "RF powering of millimeter- and submillimeter-sized neural prosthetic implants," *IEEE Trans. Biomed. Eng.*, vol. 35, no. 5, pp. 323–327, May 1988.

[6] W. H. Ko, S. P. Liang, and C. D. Fung, "Design of radio-frequency powered coils for implant instruments," *Med. Biol. Eng. Comp.*, vol. 15, pp. 634–640, 1977.

[7] I. C. Forster, "Theoretical design and implementation of transcutaneous multichannel stimulator for neural prostheses applications," *J. Biomed. Eng.*, vol. 3, pp. 107–120, Apr. 1981.

[8] N. N. Donaldson and T. A. Perkins, "Analysis of resonant coupled coils in the design of radio-frequency transcutaneous links," *Med. Biol. Eng. Comput.*, vol. 21, pp. 612–627, Sep. 1983.

[9] E. S. Hochmair, "System optimization for improved accuracy in transcutaneous signal and power transmission," *IEEE Trans. Biomed. Eng.*, vol. 31, pp. 177–186, Feb. 1984.

[10] P. E. K. Donaldson, "Frequency-hopping in R.F. energy-transfer links," *Electron. Wireless World*, pp. 24–26, Aug. 1986.

[11] C. M. Zierhofer and E. S. Hochmair, "High-efficiency coupling-insensitive transcutaneous power and data transmission via an inductive link," *IEEE Trans. Biomed. Eng.*, vol. 37, no. 7, pp. 716–722, Jul. 1990.

[12] C. M. Zierhofer and E. S. Hochmair, "Geometric approach for coupling enhancement of magnetically coupled coils," *IEEE Trans. Biomed. Eng.*, vol. 43, no. 7, pp. 708–714, Jul. 1996.

[13] T. Akin, K. Najafi, and R. M. Bradley, "A wireless implantable multichannel digital neural recording system for a micromachined sieve electrode," *IEEE J. Solid-State Circuits*, vol. 33, no. 1, pp. 109–118, Jan. 1998.

[14] W. Liu, K. Vichienchom, M. Clements, S. C. DeMarco, C. Hughes, E. McGucken, M. S. Humayun, E. de Juan, J. D. Weiland, and R. Greenberg, "A neuro-stimulus chip with telemetry unit for retinal prosthetic device," *IEEE J. Solid-State Circuits*, vol. 35, no. 10, pp. 1487–1497, Oct. 2000.

[15] C. Sauer, M. Stanaćević, G. Cauwenberghs, and N. Thakor, "Power harvesting and telemetry in CMOS for implanted devices," *IEEE Trans. Circuits Syst. I*, vol. 52, no. 12, pp. 2605–2613, Dec. 2005.

[16] M. W. Baker and R. Sarpeshkar, "Feedback analysis and design of RF power link for low-power bionic systems," *IEEE Trans. Biomed. Circuits Syst.*, vol. 1, no. 1, pp. 28–38, Mar. 2007.

[17] J. Kim and Y. Rahmat-Samii, "Implanted antennas inside a human body: Simulations, designs, and characterizations," *IEEE Trans. Microw. Theory Tech.*, vol. 52, no. 8, pp. 1934–1943, Aug. 2004.

[18] P. Soontornpipit, C. M. Furse, and Y. C. Chung, "Design of implantable microstrip antenna for communication with medical implants," *IEEE Trans. Microw. Theory Tech.*, vol. 52, no. 8, pp. 1944–1951, Aug. 2004.

[19] L. Wang, T. Drysdale, and D. R. S. Cumming, "In situ characterization of two wireless transmission schemes for ingestible capsules," *IEEE Trans. Biomed. Eng.*, vol. 54, no. 11, pp. 2020–2027, Nov. 2007.

[20] S. Soora, K. Gosalia, M. Humayun, and G. Lazzi, "A comparison of two and three dimensional dipole antennas for an implantable retinal prosthesis," *IEEE Antennas Propag.*, vol. 56, no. 3, pp. 622–629, Mar. 2008.

[21] A. V. Vorst, A. Rosen, and Y. Kotsuka, *RF/Microwave Interaction With Biological Tissues*. Hoboken-Piscataway, NJ: Wiley-IEEE Press, 2006.

[22] H. Ling, S.-W. Lee, and W. Gee, "Frequency optimization of focused microwave hyperthermia applicators," *Proc. IEEE*, vol. 72, no. 2, pp. 224–225, Feb. 1984.

[23] S. Gabriel, R. W. Lau, and C. Gabriel, "The dielectric properties of biological tissues: III. Parametric models for the dielectric spectrum of tissues," *Phys. Med. Biol.*, vol. 41, no. 11, pp. 2271–2293, Nov. 1996.

[24] IE3D Version 12.2 Zeland Software Inc.

[25] J. B. Andersen, "Theoretical limitations on radiation into muscle tissue," *Int. J. Hyperthermia*, vol. 1, no. 1, pp. 45–55, Jan. 1985.

[26] W. C. Chew, *Waves and Fields in Inhomogeneous Media*. New York: IEEE Press, 1995.

[27] J. D. Jackson, *Classical Electrodynamics*, 3rd ed. New York: Wiley, 1998.

[28] T. J. Cui and W. C. Chew, "Fast evaluation of sommerfeld integrals for EM scattering and radiation by three-dimensional buried objects," *IEEE Trans. Geosci. Remote Sensing*, vol. 37, no. 2, pp. 887–900, Mar. 1999.

Ada S. Y. Poon (S'98–M'04) received the B.Eng. and M.Phil. degrees in electrical and electronic engineering from the University of Hong Kong, in 1996 and 1997, respectively, and the M.S. and Ph.D. degrees in electrical engineering and computer sciences from the University of California at Berkeley, in 1999 and 2004, respectively.

In 2004, she was a Senior Research Scientist at Intel Corporation, Santa Clara, CA. In 2005, she was a Senior Technical Fellow at SiBeam, Inc., Fremont, CA. In 2006–2007, she was an Assistant Professor at the Department of Electrical and Computer Engineering, University of Illinois at Urbana-Champaign. Since 2008, she has been at the Department of Electrical Engineering, Stanford University, where she is currently an Assistant Professor. Her current research interests focus on the applications of electrical engineering to advance surgical instruments, and *in vivo* diagnostics and therapeutic treatments.

Stephen O'Driscoll (S'03–M'09) received the B.E. degree in electrical engineering from University College Cork, Ireland, in 2001 and the M.Sc. and Ph.D. degrees also in electrical engineering from Stanford University, Stanford, CA, in 2005 and 2009, respectively.

During 1999 and 2000, he developed an RF front end for 77 GHz radar at Farran Technology, Ballincollig, Ireland. From 2001 to 2003, he was with Cypress Semiconductor, San Jos, CA, where he worked on analog circuit design for clock and data recovery PLLs for wireline communications in both SiGe BiCMOS and CMOS processes. Since August 2009, he has been an Assistant Professor in the Department of Electrical and Computer Engineering, University of California, Davis, where his research focus is on analog and RF IC design for biomedical and other low power applications, wireless power transfer, system configured analog circuits and analog optimization tools.

Dr. O'Driscoll was a recipient of the Lu Stanford Graduate Fellowship.

Teresa H. Meng (S'82–M'83–SM'93–F'99) received the B.S. degree from National Taiwan University, and the M.S. and Ph.D. degrees in EECS from the University of California at Berkeley.

Currently, she is the Reid Weaver Dennis Professor of Electrical Engineering at Stanford University, Stanford, CA. Her research activities during the first 10 years at Stanford focused on low-power circuit and system design, video signal processing, and wireless communications. In 1999, she took leave from Stanford and founded Atheros Communications, Inc., which is a leading developer of semiconductor system solutions for wireless network communications products. She returned to Stanford University in 2000 to continue her research and teaching at the University. Her current research interests are bio-implant technologies, neural signal processing and non-invasive medical treatments using focused EM energy. She is the author of one book, several book chapters, and over 200 technical articles in journals and conferences.

Dr. Meng is a Fellow of the IEEE and a member of the National Academy of Engineering. She has received many awards and honors, including the 2009 IEEE Donald O. Pederson Award, the DEMO Lifetime Achievement Award, the McKnight Technological Innovations in Neurosciences Award in 2007, the Distinguished Lecturer Award from the IEEE Signal Processing Society in 2004, the Bosch Faculty Scholar Award in 2003, Innovator of the Year Award by MIT Sloan School eBA in 2002 and the CIO 20/20 Vision Award in 2002. She was named one of the Top 10 Entrepreneurs by Red Herring in 2001 and received a Best Paper Award from the IEEE Signal Processing Society, an NSF Presidential Young Investigator Award, an ONR Young Investigator Award, and an IBM Faculty Development Award, all in 1989, and the Eli Jury Award from U.C. Berkeley in 1988. She has given plenary talks at major conferences in the areas of signal processing and wireless communications.